THEORETICAL STUDY OF COMPLEXES OF THE TYPE $[Pt_3(M\text{-}L)_3(L`)_3]$-X (L=CO,$SO_2$,CNH; L`=PH_3,CNH; X=Tl^+, Hg^0, MPH_3^+ (M = Cu, Au, Ag))

FERNANDO MENDIZABAL[1,2], DANIELA DONOSO[1]* AND RICHARD SALAZAR[1,3]*

[1]*Departamento de Química, Facultad de Ciencias, Universidad de Chile, Casilla 653, Santiago, Chile.*
[2]*Center for the Development of Nanoscience and Nanotechnology, CEDENNA, Santiago, Chile*
[3]*Departamento de Química, Facultad de Ciencias Básicas, Universidad Metropolitana de Ciencias de la Educación, Santiago, Chile.*

ABSTRACT

The interaction between the $[Pt_3(\mu\text{-}L)_3(L`)_3]$ cluster (L = CO, $SO_2$, CNH; L` = PH_3, CNH) and a series of fragments X (Tl^+, Hg(0), $AuPH_3^+$, $CuPH_3^+$ and $AgPH_3^+$) was studied using ab initio methodology. The calculations suggest that the complexes formed are stable. We have studied these complexes at the HF, MP2, B3LYP and PBE levels of theory. The magnitude of the interaction energies and Pt_3-MPH_3^+ distances indicate a substantial covalent character of the bond. On the other hand, in $[Pt_3(\mu\text{-}L)_3(L`)_3]$-X ($Tl^+$ and Hg) the energy magnitudes are in the order of metallophilic interaction, which indicates that the dispersion and ionic terms are found as the main contribution to stability. These results have been confirmed by orbital diagrams. In addition, the Fukui index of electrophilic attack and electrophilicity index on the $[Pt_3(\mu\text{-}L)_3(L`)_3]$ clusters were used to explore possible sites that may play a role in chemical reactivity.

Keywords: Platinum clusters; metallic interactions; reactivity.

INTRODUCTION

For Biani [1] the reactivity of transition-metal cluster compounds was an area of continuing interest in organometallic chemistry, affirming that an understanding of the reactions that such systems undergo is essential for any evaluation of their potential as catalysts. Likewise, analogous complexes like Pt_3Au and Pt_3Au_2, such as $[Pt_3(\mu\text{-}CO)_3L_3\text{-}(\mu_3\text{-}AuL)]^+$ and $[Pt_3(\mu\text{-}CO)_2(\mu\text{-}SO_2)L_3\text{-}(\mu_3\text{-}AuL)]^+$ which are formed by addition of AuL^+ fragments to 42-electron or 44-electron Pt_3 clusters have been studied [2]. The units formed are stable, and may be considered to be made by donation of electron density from the HOMO of the $[Pt_3(\mu\text{-}L)_3(L`)_3]$ cluster to the vacant sp-hybrid orbital of the LAu^+ fragment.

Trimetal clusters (Pd and Pt) are susceptible to stacking containing the late transition metals [3]. Such stackable metal triangles typically have the M_3L_6, (M= Pd, Pt) stoichiometry in which three of the six L ligands are terminal (L_t) and the other three ligands (L_b) are bridge [3]. A particularly case is $[Pt_3(\mu\text{-}CO)_3(PR_3)_3]$ [4], a cluster that has both σ-donor and weak π-acceptor properties. The d^{10}-d^{10} interactions between the Pt_3 core and the coin metal have been described theoretically in the literature [5,6]. When the $[Pt_3(\mu\text{-}CO)_3(PR_3)_3]$ cluster reacts with two Hg atoms it forms a sandwich type. It can also react with donors like PR_3 and CO [7]. Thus, the reaction of $[Pt_3(\mu_2\text{-}C0)_3L_3]$ with HgI_2 can be described as a redox reaction, where a part of the platinum(0) cluster is first oxidized to Pt(I) and then to Pt(II), while Hg(II) is reduced to Hg(I).

Imhof et al. [8] synthesized a series of trinuclear platinum clusters such as $[Pt_3(\mu\text{-}CO)_3(PR_3)_3]$, $[Pt_3\text{-}(\mu\text{-}CNR)_2(\mu\text{-}CO)(CNR)(PR_3)_2]$, $[Pt_3(\mu\text{-}CNR)_3(CNR)_2(PR_3)]$, and $[Pt_3(\mu\text{-}SO_2)_3\text{-}(\mu\text{-}L)(PR_3)_3]$ (L=CNXyl, Cl, SO_2, CO). They can form heterometallic clusters by reaction with many metal-containing units, ML. The stability of the heterometallic platinum clusters can be correlated with the Lewis acidity strength of the metal cations. So the more acidic Au^+ ($pK_{hyd.} < 4$) is, the more strongly it coordinates than the less acidic Cu^+ and Ag^+ ($pK_{hyd.}$ ca. 6.9) [8]. These heterometallic clusters provide care in homogeneous and heterogeneous catalysis [9]. For example, the catalytic oxidation of carbon monoxide on a platinum surface can be modeled, in part, by platinum carbonyl clusters [10].

These systems have been studied by Extended Hückel molecular orbital theory (EHT) and ab initio calculations [11-13]. They have been analyzed from the electronic and structural properties of triangular platinum clusters [11], proposing that the cluster bonding orbitals are markedly stabilized by edge-bridging ligands. For example, in the $[Pt_3(\mu\text{-}CO)_3(PH_3)_3]$-$AuPH_3^+$ models, the $AuPH_3^+$ fragments cap the Pt_3 triangles by utilising the acceptor orbital of a_1 symmetry localized on gold [12,13]. We have predicted stable triplatinum clusters with fragments of the type MPH_3^+ (M = Cu^+, Ag^+, Au^+) in $[Pt_3(CO)_3(PH_3)_3\text{-}M(PH_3)]^+$ [14]. The Pt_3–M distances indicate a substantial covalent character of the bond. The charge transfer is mainly due to the carbonyl and the phosphine, while platinum atoms and electrophiles receive charge.

The interest of this work is to extend the type of platinum cluster and quantify the effect of the ligands that form such clusters. For this purpose, we studied the structure, binding properties and reactivity of the following triangular platinum clusters: $[Pt_3(L)_3(L`)_3\text{-}M(PH_3)]^+$ with M=Cu, Ag, Au and L=CO, $PH_3$, CNH; and $[Pt_3(L)_3(L`)_3\text{-}M]$ with M=Tl^+,Hg(0) and L=CO, PH_3, CNH. In addition, we propose to study on site basicity using frontier orbitals, applying reactivity indices as introduced through conceptual density functional theory (CDFT) [15,16].

Models and Computational Methods

A simplified model of the experimental structures with general formula $[Pt_3(\mu\text{-}L)_3(L')_3]$-$MPH_3^+$ and $[Pt_3(\mu\text{-}L)_3(L')_3]$–X (L = PH_3; SO_2, CNH; L' = PH_3; CNH) are depicted in Figures 1 and 2. In order to keep the computation feasible, we use phosphine (PH_3) instead of the original triphenylphosphine (PPh_3) and tricyclohexylphosphine (PCy_3) ligands.

The theoretical studies have been carried out by ab initio calculations available in the Gaussian03 program [17] at the Hartree-Fock (HF), second-order Møller-Plesset perturbation theory (MP2) [18], B3LYP and PBE [19]. For the heavy elements Pt, Au, Ag and Cu, the Stuttgart small-core quiasirelativistic effective core pseudopotentials (PP) were used: 18 valence-electrons (VE) for Pt and 19 for Au, Ag and Cu [20]. Two *f*-type polarization functions were added: Pt (a_f= 0.70, 0.14), Au (α_f = 0.20, 1.19), Ag (α_f = 0.22, 1.72) and Cu (a_f = 0.24, 3.70) [21]. The C, O and P atoms were also treated with PP, using a double-zeta basis set and adding one *d*-type polarization function [22]. For hydrogen, a valence-double-zeta basis set with one *p*-polarization function was used [23].

The counterpoise correction for the basis-set superposition error (BSSE) was used for the calculated interaction energies [24]. This correction is estimated as the difference between the energies of the whole system and its fragments. We have fully optimized the geometry of the model for each one of the methods mentioned above.

To predict the reactivity of the systems, using the frontier orbital analysis [15,16], applying the conceptual density functional theory (CDFT) [25-29], analyzing properties such as hardness (2) and the chemical potential (3).

With the aim of understanding the interaction of the electrophilic fragments MPH_3^+ (M = Au, Ag, Cu) and X (Tl^+, Hg) with the $[Pt_3(\mu\text{-}L)_3(L')_3]$ (L = PH_3; SO_2, CNH; L' = PH_3; CNH) clusters, we have used the CDFT, the electronic chemical potential (μ), and chemical hardness (η) from operational DFT [28,29], which are defined as:

$$\mu \approx -\frac{(IP + EA)}{2} \quad (1)$$

$$\eta \approx \frac{(IP - EA)}{2} \quad (2)$$

e-mail: hagua@uchile.cl

where IP is the ionization potential and EA is the electron affinity. These two quantities can also be defined based on orbitals; on the basis of Koopmans' theorem as IP ≈ $-E_{HOMO}$ and EA ≈ $-E_{LUMO}$, where E_{HOMO} and E_{LUMO} are the energies of the highest occupied molecular orbital (HOMO) and lowest unoccupied molecular orbital (LUMO), respectively. On the other hand, the electrophilicity index (ω) is defined as [25]

$$\omega = \frac{\mu^2}{2\eta} (3)$$

which is a measure of the electrophilicity of the molecule or fragment, and corresponds to a measure of the second-order energy of an electrophile when it gets saturated with electrons [26]. The higher its value, the greater is the electrophilic capacity. In addition, to see reactive sites, the local orbital Fukui function [30] for the nucleophilic cluster was determined from its frontier orbital density at atom *M,* where *M* represents a metal atom like platinum. The orbital Fukui function at the platinum atom for electrophilic attack is given as

$$f_{Pt}^{\alpha} = \sum_{\nu \in M}^{AO} C_{\nu\alpha}^2 + \sum_{\chi \neq \nu}^{AO} C_{\chi\alpha} C_{\nu\chi} S_{\nu\chi} \quad (4)$$

where α = - for HOMO, $C_{\nu\alpha}$ are the molecular orbital frontier coefficients (HOMO), and $S_{\nu\chi}$ are the atomic orbital overlap matrix elements. This definition of the orbital Fukui function has been used in several studies, yielding reliable results [31,32]. Moreover, a local electrophilicity has been introduced to analyze the electrophile-nucleophile reactions. It is defined as

$$\omega_{Pt}^{-} = \omega f_{Pt}^{-} (5)$$

An analysis of electrophilicity on platinum atom (ω_{Pt}^{-}) provides the local information in a molecule being attacked by an electrophile fragment [33] .

RESULTS AND DISCUSSION

We show the results divided into two groups of electrophiles, MPH_3^+ and M. Subsequently, we focus attention on the properties as base for the $[Pt_3(\mu\text{-}L)_3(L')_3]$ clusters.

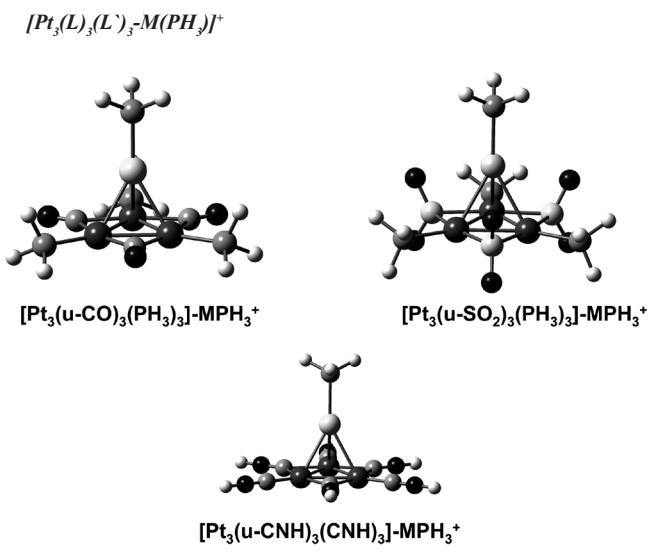

Figure 1. The $[Pt_3(\mu\text{-}CO)_3(PH_3)_3]$-$MPH_3^+$, $[Pt_3(\mu\text{-}SO_2)_3(PH_3)_3]$-$MPH_3^+$, and $[Pt_3(\mu\text{-}CNH)_3(CNH)_3]$-$MPH_3^+$ (M =Au, Ag, Cu) models.

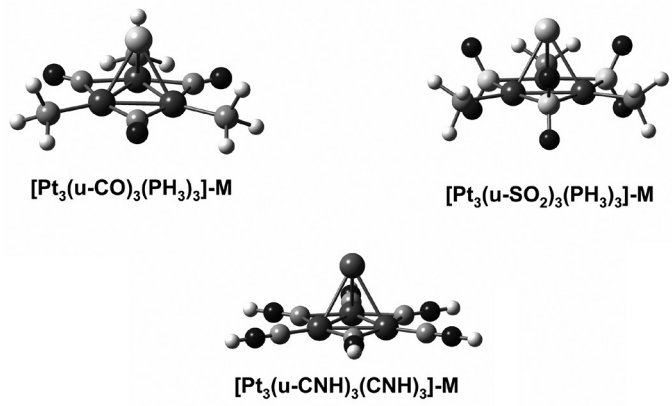

Figure 2. The $[Pt_3(\mu\text{-}CO)_3(PH_3)_3]$-X, $[Pt_3(\mu\text{-}SO_2)_3(PH_3)_3]$-X, and $[Pt_3(\mu\text{-}CNH)_3(CNH)_3]$-X (X = Hg, Tl(I)) models.

Tables 1-4 summarize the main geometric parameters and interaction energies obtained for the optimized geometries at the HF, MP2, B3LYP and PBE levels. The solid-state X-ray experimental values are included as a reference for the $[Pt_3(\mu\text{-}L)_3(L')_3]$ clusters. The MP2 magnitudes are the shortest, followed by B3LYP and PBE; and the longest is HF. The complexes formed are described in Tables 2 to 4. From the Pt-M distances and the interaction energy, it is clear that electronic correlation effects play an important role in the stability of the system (HF between 271.0 pm and 304.2 pm). The Pt-M distances obtained with all methods are close to those of a typical single bond of the experimental structures [34-37], with the shortest distance obtained with the MP2 method as indicated by the literature [6], and the same goes for the Pt-Pt, Pt-P and M-P distances. For example, the Pt-P distances in the $[Pt_3(\mu\text{-}CO)_3(PH_3)_3]$ complex is nearly 227 pm, which increases slightly when the cluster is formed (229 pm) [34]. We see the same behavior on a theoretical level in Tables 2-4. In the case of Ag-P, the distances of the electrophile (Tables 2-4) decrease slightly at all theoretical levels when the complex is formed (239.2 pm). Also, the H-Pt-P angles show less deviation compared with the free $[Pt_3(\mu\text{-}CO)_3(PH_3)_3]$ complex.

The magnitude of the interaction energy obtained varies for each complex. It is generally associated with a covalent bond [34], so for gold it is between 136.9 kJ/mol HF (SO_2) and 492 kJ/mol MP2 (CO); for silver, between 107.7 kJ/mol HF (SO_2) and 411.0 kJ/mol MP2 (CO); for copper, between 131.3 kJ/mol HF (SO2) and 421.5 kJ/mol MP2 (CO) depending on the method, fragment and cluster used. We can see that there is orbital stabilization due to the formation of stable adducts between the $[Pt_3(\mu\text{-}CO)_3(PH_3)_3]$ or $[Pt_3(\mu\text{-}SO_2)_3(PH_3)_3]$ or $[Pt_3(\mu\text{-}CNH)_3(CNH)_3]$ and the $[MPH_3]^+$ fragments.

Through the interaction energy the electronic correlation was also analyzed, since the complexes show a strong oscillation of such energy. Depending on the method used, it is seen that all complexes are already stabilized at the HF level, as shown in Table 2-4. It is clear that the electronic correlation component plays an important role. When the electronic correlation is included, increased interaction energy is obtained.

In order to get a better insight into such stabilization, we have depicted in Figure 3 the orbital energies for $[Pt_3(\mu\text{-}CNH)_3(CNH)_3]$-$MPH_3^+$ at the MP2 level. In the three complexes the electronic levels are very similar because the fragments are isolobal [15]. The frontier molecular orbital positions in the orbital energy spectra of the three complexes have a HOMO-LUMO gap of approximately 5.9 eV for all the complexes. They have the same number of bonding orbitals, and similar but not necessarily identical shapes and symmetries. This is repeated for the other Pt_3 clusters (not shown here).

With the purpose of studying the formation of the bonds between $[Pt_3(\mu\text{-}L)_3(L')_3]$ and MPH_3^+, we propose an interaction diagram for the frontier molecular orbitals. The $[Pt_3(\mu\text{-}CNH)_3(CNH)_3]$ and $CuPH_3^+$ fragments are used. Similar results were obtained for $AgPH_3^+$ and $AuPH_3^+$. Figure 4 shows the left and right sides corresponding to the frontier levels of the platinum complex and $CuPH_3^+$, respectively. The center of the diagram corresponds to the molecular orbitals for the $[Pt_3(\mu\text{-}CNH)_3(CNH)_3]$-$CuPH_3^+$ complex. Six orbitals show a strong interaction: $56a_1$, $62a_1$, $65a_1$, $81a_1$, $84a_1$ and $85a_1$, whereas the molecular orbitals remain unchanged. The orbitals generate the bonding ($56a_1$, $62a_1$, $65a_1$) and antibonding ($81a_1$, $84a_1$, $85a_1$) sigma levels from dp_xp_y to dsp* (Pt) and from d to sp_z* (Cu). These results clearly indicated a net effect of bonding through the orbital interactions. This magnitude is associated with covalent bonds.

Table 1. Main geometric parameters of the $[Pt_3(\mu\text{-}L)_3(L')_3]$ (L = CO, SO_2, CNH; L´ = PH_3, CNH) clusters (distances in pm and angles in degrees) at different levels of calculation.

Cluster	Method	Pt-Pt	Pt-L`	Pt-L	Pt-Pt-Ptº	L-Pt-Ptº
$[Pt_3(\mu\text{-}CO)_3(PH_3)_3]$	HF	273.7	233.7	212.6	60.0º	49.9º
	MP2	262.0	226.1	207.0	60.0º	50.7º
	B3LYP	271.3	230.8	210.2	60.0º	49.8º
	PBE	268.7	228.8	208.4	60.0º	49.9º
$[Pt_3(\mu\text{-}SO)_3(PH_3)_3]$	HF	275.7	236.6	233.2	60.0º	53.8º
	MP2	267.0	228.5	231.9	60.0º	54.8º
	B3LYP	277.0	233.4	235.3	60.0º	53.9º
	PBE	274.7	231.2	234.3	60.0º	54.2º
$[Pt_3(\mu\text{-}CNH)_3(CNH)_3]$	HF	276.8	197.0	215.3	60.0º	49.9º
	MP2	266.3	188.4	209.0	60.0º	50.4º
	B3LYP	275.6	192.2	212.6	60.0º	49.6º
	PBE	273.5	190.1	210.4	60.0º	49.5º
$[Pt_3(\mu\text{-}CO)_3(PCy_3)_3]$[a] [3]	Exp	265.4	227.5	206.3	60.0º	50.6º
$[Pt_3(\mu\text{-}SO_2)_3(PCy_3)_3]$[a] [36]	Exp	281.4	228.7	227.1	60.0º	51.4º
$[Pt_3(\mu\text{-}CNBu)_3(CNBu)_3]$[b] [41]	Exp	263.2	190.3	208.3	60.0º	50.9º

[a]PCy_3 = tricyclohexylphosphine.
[b]Bu = butyl.

Table 2. Main geometric parameters of the $[Pt_3(\mu\text{-}CO)_3(PH_3)_3]$-$MPH_3^+$ complex (M =Au, Ag, Cu). Distances in pm and angles in degrees at different levels of calculation. The interaction energy $V(R_e)$ is shown with BSSE (kJ/mol).

System	Method	Pt-M	Pt-Pt	Pt-P	C-O	M-P	H-P-Ptº	P-M-Ptº	$V(R_e)$
$[Pt_3(\mu\text{-}CO)_3(PH_3)_3]$-$AuPH_3^+$	HF	291.3	275.3	237.1	112.4	238.6	117.7	117.8	-199.9
	MP2	269.8	263.0	228.5	117.1	225.7	117.4	116.8	-492.6
	B3LYP	284.9	273.3	233.7	115.7	231.8	117.2	117.3	-268.3
	PBE	281.2	270.8	231.7	117.1	229.4	118.4	123.8	-309.3
$[Pt_3(\mu\text{-}CO)_3(PH_3)_3]$-$AgPH_3^+$	HF	295.4	274.9	236.8	112.5	260.5	117.8	117.8	-162.5
	MP2	270.3	262.8	228.6	117.3	234.5	117.5	118.0	-411,0
	B3LYP	285.6	273.1	233.7	115.9	243.6	118.3	118.4	-230.9
	PBE	281.5	270.7	231.7	117.2	238.7	118.5	118.8	-265.9
$[Pt_3(\mu\text{-}CO)_3(PH_3)_3]$-$CuPH_3^+$	HF	273.8	274.9	237.1	112.4	238.7	117.8	117.7	-190.8
	MP2	253.3	262.3	228.9	117.2	212.7	117.4	118.1	-421.5
	B3LYP	272.9	264.5	233.8	115.7	222.7	118.2	118.3	-268.6
	PBE	260.9	270.3	231.8	117.2	219.7	118.4	118.7	-309.6
$[Pt_3(\mu\text{-}CO)_3(PCy_3)_3]$-$AuPCy_3^+$ [7]	Exp	275.8	270.8	227.3		227.0			
$[Pt_3(\mu\text{-}CO)_3(PPh_3)_3]_2$-$Au^+$ [7]	Exp	272.8	268.3						
$[Pt_3(\mu\text{-}CO)_3(PPh_3)_3]_2$-$Ag^+$ [8]	Exp	283.6	266.6						
$[Pt_3(\mu\text{-}CO)_3(P^iPr_3)_3]$-$CuP^iPr_3^+$[a] [8]	Exp	260.4	267.1						

[a]P^iPr_3 is tribulkyphosphine.

Table 3. Main geometric parameters of the $[Pt_3(\mu\text{-}CNH)_3(CNH)_3]\text{-}MPH_3^+$ complex (M =Au, Ag, Cu). Distances in pm and angles in degrees at different levels of calculation. The interaction energy $V(R_e)$ is shown with BSSE (kJ/mol).

System	Method	Pt-M	Pt-Pt	Pt-C	N-H	M-P	P-M-Pt°	$V(R_e)$
$[Pt_3(\mu\text{-}CNH)_3(CNH_3)_3]\text{-}AuPH_3^+$	HF	288.9	277.7	200.8	99.1	237.7	146.3	-284.6
	MP2	269.4	266.1	190.7	100.8	225.1	145.2	-447.5
	B3LYP	283.8	276.6	194.8	100.5	231.3	145.8	-341.6
	PBE	280.1	274.5	192.4	101.1	228.7	145.5	-374.6
$[Pt_3(\mu\text{-}CNH)_3(CNH_3)_3]\text{-}AgPH_3^+$	HF	292.0	277.5	200.6	99.1	261.1	146.7	-245.9
	MP2	269.8	266.0	190.6	100.7	233.9	145.3	-364.4
	B3LYP	284.2	276.3	194.8	100.5	243.0	145.9	-301.5
	PBE	280.4	274.2	192.4	101.1	238.1	145.6	-331.7
$[Pt_3(\mu\text{-}CNH)_3(CNH_3)_3]\text{-}CuPH_3^+$	HF	271.0	277.3	200.7	99.1	238.5	143.8	-279.4
	MP2	252.9	265.2	191.1	100.8	212.0	142.7	-397.2
	B3LYP	263.3	276.2	194.9	100.5	222.1	142.7	-350.4
	PBE	260.3	274.2	192.5	101.1	219.1	142.5	-378.7
$[Pt_3(\mu\text{-}CNXyl)_3(CNXly)_2(PCy_3)][AuPCy_3]$[a] [35]	Exp	277.8	266.9	198.3		225.7		

[a]CNXyl is isocyanide.

Table 4. Main geometric parameters of the $[Pt_3(\mu\text{-}SO_2)_3(PH_3)_3]\text{-}MPH_3^+$ complex (M =Au, Ag, Cu). Distances in pm and angles in degrees at different levels of calculation. The interaction energy $V(R_e)$ is shown with BSSE (kJ/mol).

System	Method	Pt-M	Pt-Pt	Pt-P	Pt-S	M-P	H-P-Pt°	P-M-Pt°	$V(R_e)$
$[Pt_3(\mu\text{-}SO_2)_3(PH_3)_3]\text{-}AuPH_3^+$	HF	296.7	278.7	238.5	234.5	239.0	116.1	147.2	-136.9
	MP2	270.7	268.3	230.3	233.7	226.2	116.1	145.1	-465.7
	B3LYP	287.1	280.1	235.4	237.3	232.5	116.7	145.7	-234.2
	PBE	282.5	277.2	233.3	236.4	230.0	117.0	145.5	-269.7
$[Pt_3(\mu\text{-}SO_2)_3(PH_3)_3]\text{-}AgPH_3^+$	HF	304.2	277.9	238.6	234.0	260.5	116.2	148.2	-107.7
	MP2	271.1	267.8	230.4	232.9	235.4	116.1	145.2	-392.2
	B3LYP	288.8	279.6	235.6	236.7	244.4	116.8	146.0	-201.2
	PBE	283.4	276.8	233.4	235.8	239.7	117.0	145.7	-229.9
$[Pt_3(\mu\text{-}SO_2)_3(PH_3)_3]\text{-}CuPH_3^+$	HF	280.0	277.5	238.8	234.1	238.1	116.1	145.1	-131.3
	MP2	254.5	267.6	230.7	233.3	214.0	116.0	142.6	-394.5
	B3LYP	267.3	279.3	235.6	236.9	223.0	116.7	142.8	-233.4
	PBE	263.2	276.7	233.5	236.1	220.4	117.0	142.6	-272.7
$[Pt_3(\mu\text{-}SO_2)_2(\mu\text{-}Cl)(PCy_3)_3][AuPPh_3]^+$ [37]	Exp	278.5	288.6	231.2	232.0	224.6			
$[Pt_3(\mu\text{-}SO_2)_2(\mu\text{-}Cl)(PPh_3)_3]$ $[AuPPh_3]^+$ [37]	Exp	276.8	286.4	228.5	227.8	225.8			

[a]PPh_3 is triphenylphosphine.

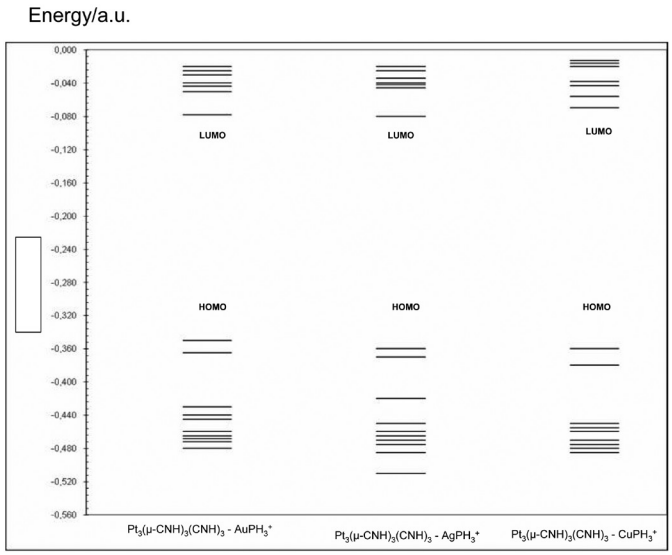

Figure 3. The orbital energy of $[Pt_3(\mu\text{-}CNH)_3(CNH)_3]\text{-}MPH_3^+$ (M = Au, Ag, Cu).

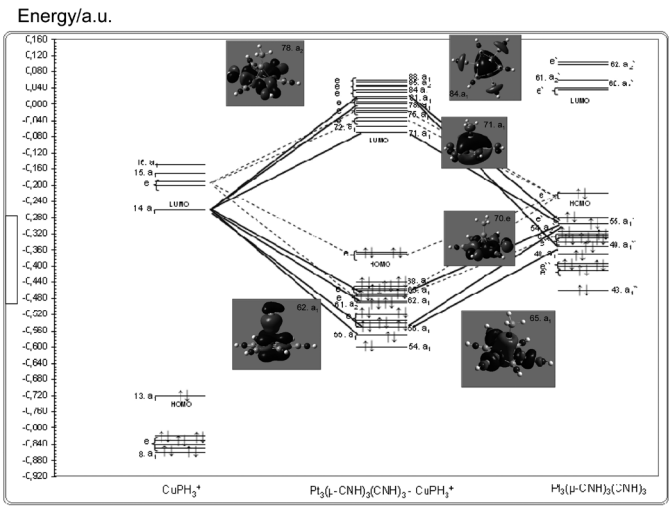

Figure 4. Orbital energy diagram for the $[Pt_3(\mu\text{-}CNH)_3(CNH)_3]\text{-}CuPH_3^+$ complex.

Table 5 shows the natural bond orbital (NBO) population analysis [38] based on the MP2 density of the complexes. Where atomic charges can be distinguished we see that the Au charge (+0.363) in the $[Pt_3(\mu\text{-}CNH)_3(CNH)_3]\text{-}AuPH_3^+$ system decreases compared to the Au-free electrophilic $AuPH_3^+$ (+0.646), which indicates that Au is accepting electrons from the flow of C. The Pt charge (-0.325) in the system decreases compared to the free $[Pt_3(\mu\text{-}CNH)_3(CNH)_3]$ (+0.140) cluster, where Pt is gaining electrons. A similar situation is seen when the electrophiles are Cu and Ag. The charge is transferred from the $[Pt_3(\mu\text{-}CNH)_3(CNH)_3]$ system to the MPH_3^+ fragment in the $[Pt_3(\mu\text{-}CNH)_3(CNH)_3]\text{-}MPH_3^+$ complex. The charge flow comes from the carbonyls and nitrogen, and is greater when the electrophile is the Cu fragment, followed by Ag and finally Au. The gross population per atom shell shows changes in the bond between the metal fragments due to electron transfer. Thus, real effect is an inductive charge transfer where the electrophilic unit withdraws charge from the Pt_3 core. The Pt_3 core then compensates for the electron deficiency by pulling charge from the ligands. The situation is similar for complexes $[Pt_3(\mu\text{-}CO)_3(PH_3)_3]\text{-}MPH_3^+$ and $[Pt_3(\mu\text{-}SO_2)_3(PH_3)_3]\text{-}MPH_3^+$ (not shown here).

$Pt_3(L)_3(L`)_3$]-X

The results of our calculations (see Table 6) supports the proposed original idea that the $[Pt_3(L)_3(L`)_3]$ systems show different interactions with Hg and Tl^+ at the MPH_3^+ fragments of the section above. Concerning the Pt-M distances and the interaction energies, it is clear that electronic correlation effects play an important role in the stability of the systems. The Pt-X distances obtained with all methods show oscillations; however, the distances obtained with the MP2 method are the shortest. It is worth noting that the MP2 approximation overestimates the metallic interactions [6]. The distances obtained in this work indicates that the Pt$\cdots$X (X = Hg(0), Tl(I)) contact is a strong closed-shell interaction, which goes beyond the classic metallophilic interaction. Such distances are within the experimental range [39,40].

The magnitude of the interaction energies obtained varies according to the method used and the system studied. Thus, for $[Pt_3(L)_3(L`)_3]$-Hg complexes we can see that the interaction energies at the HF level are practically zero. The complexes do not show stable interaction energies. However, the results at the MP2 level are all attractive in the range of van der Waals interactions between 88.0 kJ/mol and 61.8 kJ/mol. The two methods at the DFT levels (B3LYP and PBE) get some attraction. The interaction energy is greater with PBE because this method includes some electronic correlation.

On the other hand, in the $[Pt_3(L)_3(L`)_3]\text{-}Tl^+$ complexes the interaction energies are closer to a formal Pt-Tl bond. For these systems this might be indicative of an orbital stabilization due to the formation of stable adducts between the Pt_3 core and the thallium cation. There are strong oscillations in the magnitudes of the interaction energies. This behavior was previously seen in complexes of the $[Pt(PH_3)_3]\text{-}Tl^+$ type. The thallium complexes show interaction energies greater than the mercury complexes because the terms of charge-induced dipole and dispersion terms are added. The interaction energy obtained varies, depending on the method used, between 93.7 kJ/mol (HF) and 367 kJ/mol (MP2). The complex is already stabilized at the HF level as seen in Table 6.

The natural bond orbital (NBO) population analysis for the complexes is shown in Table 7. This analysis is based on the MP2 density. Table 7 shows a charge transfer from the Hg and much less from Tl toward the $[Pt_3(\mu\text{-}CO)_3(PH_3)_3]$ complex (0.6721e and 0.0167e), respectively, in the $[Pt_3(\mu\text{-}CO)_3(PH_3)_3]\text{-}X$ complexes (X = Hg,Tl(I)). Platinum shows variability in its charge. The gross population per atom shell shows that for the 6p orbital (0.33e) belonging to thallium takes advantage of this charge transfer by increasing its occupation. On the contrary, the charge of the 6s orbital does not change, retaining its inert character. For mercury the situation is analogous to the 6s orbital.

Reactivity of electrophilic clusters

Using the CDFT, the global and local properties were obtained from Eqs. 1-5 for the $[Pt_3(L)_3(L`)_3]$ complexes. We summarize the results in Table 8. The electronic chemical potential and hardness are computed from ionization energy and electron affinity, with those at the ab initio level (HF and MP2) better than those at the DFT level (B3LYP and PBE). It is known that in calculations with DFT the electron density decays faster than at the ab initio level [33]. This is manifested in the μ and η values in Table 8. This effect is seen in all the clusters. However, regardless of the cluster, the trend is maintained. Also, this is obtained for the electrophilicity index (ω) values.

The local reactivity of clusters has been studied using the local orbital electrophilic Fukui function on platinum (f^-_{Pt}). In all the clusters the highest value for the electrophilic Fukui function is expected to be at the platinum atoms. Low values are expected at the other atoms. For clarity, we have not included the values of f^-_k for the other atoms of each cluster. The results are summarized in Table 8. For comparison, in general for all methods the same trend is found: $[Pt_3(\mu\text{-}SO_2)_3(PH_3)_3] > [Pt_3(\mu\text{-}CO)_3(PH_3)_3] > [Pt_3(\mu\text{-}CNH)_3(CNH)_3]$. However, the values are small and difficult to discriminate. When we used the local electrophilicity index on the platinum atoms (ω_{Pt}^-) (Table 8), we could better discriminate local properties. We have emphasized that the global variation in the electrophilicity index is modulated through the local variations being mapped at the more reactive site, as indicated through the Fukui function [30] using the ω_{Pt}^-. This means that the variation of the electrophilic index is directed to the sites where the Fukui function for electrophilic attacks is important. For comparison, the same trend is found for all methods and fragments: $[Pt_3(\mu\text{-}SO_2)_3(PH_3)_3] > [Pt_3(\mu\text{-}CO)_3(PH_3)_3] > [Pt_3(\mu\text{-}CNH)_3(CNH)_3]$. Values are larger compared to f^-_{Pt} and much easier to discriminate, although the trend is the same.

The electronic descriptors are inversely related to the magnitude of the interaction energies from MPH_3^+ electrophiles. This same trend is found for the Tl. In the case of Hg it is less clear due to the weak interaction with the Pt_3 core in the three systems studied. When we have used the electrophilicity index on platinum atom, there is a very good correlation between lower value of ω_{Pt}^- with high formation interaction energies for the respective complexes. This result reveals the character of the Platinum atom in the studied clusters.

Table 5. NBO analysis of the MP2 density for $[Pt_3(\mu\text{-}CNH)_3(CNH)_3]\text{-}MPH_3^+$, $[Pt_3(\mu\text{-}CNH)_3(CNH)_3]$ and MPH_3^+ complexes(M = Au, Ag, Cu).

System	atom	natural	natural electron configuration
$[Pt_3(\mu\text{-}CNH)_3(CNH)_3]\text{-}AuPH_3^+$	Au	+0.363	$6s^{0.59}\ 5d^{9.82}\ 6p^{0.10}\ 7p^{0.14}$
	Pt	-0.325	$6s^{0.53}\ 5d^{9.18}\ 6p^{0.06}\ 5f^{0.01}\ 7p^{0.56}$
	P	+0.260	$3s^{1.36}\ 3p^{3.31}\ 3d^{0.05}\ 4p^{0.01}$
	C	+0.533	$2s^{1.17}\ 2p^{2.24}\ 3s^{0.03}\ 3p^{0.02}\ 3d^{0.01}$
	N	-0.720	$2s^{1.30}\ 2p^{4.41}$
	C N	+0.390 -0.741	$2s^{1.11}\ 2p^{2.45}\ 3s^{0.02}\ 3p^{0.02}\ 3d^{0.01}$ $2s^{1.28}\ 2p^{4.45}\ 3p^{0.01}$
$[Pt_3(\mu\text{-}CNH)_3(CNH)_3]\text{-}AgPH_3^+$	Ag	+0.538	$5s^{0.33}\ 4d^{9.92}\ 5p^{0.10}\ 6p^{0.13}\ 6d^{0.01}$
	Pt	-0.329	$6s^{0.54}\ 5d^{9.19}\ 6p^{0.38}\ 5f^{0.01}\ 7p^{0.22}$
	P	+0.139	$3s^{1.41}\ 3p^{3.39}\ 3d^{0.04}\ 4p^{0.01}$
	C	+0.533	$2s^{1.17}\ 2p^{2.24}\ 3s^{0.03}\ 3p^{0.02}\ 3d^{0.01}$
	N	-0.723	$2s^{1.30}\ 2p^{4.41}$
	C N	+0.381 -0.743	$2s^{1.11}\ 2p^{2.46}\ 3s^{0.02}\ 3p^{0.02}\ 3d^{0.01}$ $2s^{1.28}\ 2p^{4.45}\ 3p^{0.01}$
$[Pt_3(\mu\text{-}CNH)_3(CNH)_3]\text{-}CuPH_3^+$	Cu	+0.486	$4s^{0.33}\ 3d^{9.93}\ 4p^{0.26}$
	Pt	-0.324	$5d^{9.19}\ 6p^{0.05}\ 7s^{0.54}\ 5f^{0.01}\ 7p^{0.55}$
	P	+0.169	$3s^{1.40}\ 3p^{3.37}\ 3d^{0.04}\ 4p^{0.01}$
	C	+0.534	$2s^{1.17}\ 2p^{2.24}\ 3S^{0.03}\ 3p^{0.02}\ 3d^{0.01}$
	N	-0.720	$2s^{1.30}\ 2p^{4.41}$
	C N	+0.380 -0.740	$2s^{1.11}\ 2p^{2.46}\ 3s^{0.02}\ 3p^{0.02}\ 3d^{0.01}$ $2s^{1.28}\ 2p^{4.45}\ 3p^{0.01}$
$[Pt_3(\mu\text{-}CNH)_3(CNH)_3]$	Pt	+0.140	$5d^{9.19}\ 7s^{0.64}\ 6d^{0.01}$
	C	+0.365	$2s^{1.30}\ 2p^{2.27}\ 3s^{0.03}\ 3p^{0.02}\ 3d^{0.01}$
	N	-0.789	$2s^{1.30}\ 2p^{4.48}\ 3s^{0.01}$
	C N	+0.158 -0.804	$2s^{1.25}\ 2p^{2.52}\ 3s^{0.02}\ 3p^{0.03}\ 3d^{0.01}$ $2s^{1.28}\ 2p^{4.51}\ 3p^{0.01}$
$AuPH_3^+$	Au	+0.646	$6s^{0.47}\ 5d^{9.88}$
	P	+0.169	$3s^{1.38}\ 3p^{3.37}\ 4s^{0.01}\ 3d^{0.06}\ 4p^{0.02}$
$AgPH_3^+$	Ag	+.859	$5s^{0.17}\ 4d^{9.97}\ 7p^{0.01}$
	P	-0.101	$3s^{1.44}\ 3p^{3.49}\ 4s^{0.01}\ 3d^{0.05}\ 4p^{0.02}$
$CuPH_3^+$	Cu	+0.829	$4s^{0.20}\ 3d^{9.96}\ 5p^{0.01}$
	P	+0.009	$3s^{1.43}\ 3p^{3.48}\ 4s^{0.01}\ 3d^{0.05}\ 4p^{0.01}$

Table 6. Main geometric parameters of the $[Pt_3(\mu\text{-}CO)_3(PH_3)_3]$-X, $[Pt_3(\mu\text{-}SO_2)_3(PH_3)_3]$-X and $[Pt_3(\mu\text{-}CNH)_3(CNH_3)_3]$-X complexes (X =Hg, Tl^+). Distances in pm and angles in degrees at different levels of calculation. The interaction energy $V(R_e)$ is shown with BSSE (kJ/mol).

System	Method	Pt-X	Pt-Pt	Pt-P	C-O	P-H	H-P-Pt°	$V(R_e)$
$[Pt_3(\mu\text{-}CO)_3(PH_3)_3]$-$Tl^+$	HF	310.3	274.8	237.0	112.3	140.8	117.6	-155.2
	MP2	284.1	261.7	229.1	117.1	141.6	117.2	-264.5
	B3LYP	304.7	272.2	234.1	115.7	142.6	118.0	-198.5
	PBE	300.6	269.4	232.0	117.1	144.0	118.2	-226.9
$[Pt_3(\mu\text{-}CO)_3(PH_3)_3]$-Hg	HF	416.2	273.6	233.8	113.0	141.1	118.8	-0.5
	MP2	285.8	260.9	225.8	117.7	142.0	118.7	-88.0
	B3LYP	325.3	271.0	230.8	116.3	143.0	119.4	-16.5
	PBE	315.0	268.3	228.8	117.7	144.5	119.7	-37.6
System	**Method**	**Pt-X**	**Pt-Pt**	**Pt-C**	**N-H**	**MPtC°**	**P-M-Pt°**	**$V(R_e)$**
$[Pt_3(\mu\text{-}CNH)_3(CNH_3)_3]$-$Tl^+$	HF	303.2	277.0	201.0	99.1	121.8	180.0	-261.0
	MP2	283.4	264.6	191.2	100.8	122.6	180.0	-367.7
	B3LYP	302.0	275.8	195.4	100.4	121.8	180.0	-282.9
	PBE	299.0	273.4	212.8	101.0	121.9	180.0	-305.1
$[Pt_3(\mu\text{-}CNH)_3(CNH_3)_3]$-Hg	HF	404.6	276.6	197.2	100.2	113.2	180.0	-2.1
	MP2	286.9	265.0	188.3	100.3	122.2	180.0	-73.1
	B3LYP	333.8	275.2	192.3	100.1	118.4	180.0	-13.9
	PBE	315.4	273.3	190.2	100.7	120.0	180.0	-33.0
System	**Method**	**Pt-X**	**Pt-Pt**	**Pt-P**	**Pt-S**	**O-S**	**O-S-Pt°**	**$V(R_e)$**
$[Pt_3(\mu\text{-}SO_2)_3(PH_3)_3]$-$Tl^+$	HF	318.1	278.5	235.9	296.8	149.6	101.2	-93.7
	MP2	289.1	266.7	231.2	233.8	150.0	114.5	-239.0
	B3LYP	309.7	275.6	233.8	235.9	151.4	114.3	-189.0
	PBE	335.9	277.3	238.5	233.9	145.0	114.5	-96.4
$[Pt_3(\mu\text{-}SO_2)_3(PH_3)_3]$-Hg	HF	351.4	276.8	233,4	235.9	150.1	115.2	-1.7
	MP2	291.3	265.8	228.3	233.5	150.5	115.4	-61.8
	B3LYP	324.9	274.2	231.2	235.3	151.8	115.2	-8.4
	PBE	469.0	275.7	236.6	233.2	145.5	115.2	-18.7
$[Pt_3(\mu\text{-}CO_2)_3(PCy_3)_3]$-$Tl^+$ [39]	Exp	303.9						
$[Pt_3(\mu\text{-}CO_2)_3(PPh\text{-}i\text{-}Pr_2)_3]_2$-Hg [40]	Exp	300.8						

Table 7. NBO analysis of the MP2 density for $[Pt_3(\mu\text{-}CO)_3(PH_3)_3]$-X, $[Pt_3(\mu\text{-}CO)_3(PH_3)_3]$ and X complexes (X = Hg, Tl^+).

System	atom	natural	natural electron configuration
$[Pt_3(\mu\text{-}CO)_3(PH_3)_3]$-$Tl^+$	Tl	+0.9833	$6s^{1.69}\ 6p^{0.33}\ 7s^{0.01}\ 5f^{0.10}\ 6d^{0.03}\ 7p^{0.03}$
	Pt	-0.6504	$6s^{0.69}\ 5d^{8.97}\ 6p^{0.80}\ 7s^{0.01}\ 5f^{0.11}\ 6d^{0.08}\ 7p^{0.02}$
	P	+0.4184	$3s^{1.29}\ 3p^{3.20}\ 3d^{0.07}\ 4p^{0.02}$
	C	+0.4590	$2s^{1.09}\ 2p^{2.36}\ 3s^{0.02}\ 3p^{0.05}\ 3d^{0.02}$
	O	-0.3652	$2s^{1.67}\ 2p^{4.63}\ 3p^{0.03}\ 3d^{0.03}$
$[Pt_3(\mu\text{-}CO)_3(PH_3)_3]$-Hg	Hg	+0.3279	$6s^{1.58}\ 5d^{9.98}\ 6p^{0.12}$
	Pt	-0.6145	$6s^{0.55}\ 5d^{9.30}\ 6p^{0.77}\ 5f^{0.01}$
	P	+0.4664	$2s^{1.68}\ 2p^{4.90}\ 3p^{0.01}\ 3d^{0.02}$
	C	+0.6605	$2s^{1.13}\ 2p^{2.14}\ 3s^{0.02}\ 3p^{0.04}3d^{0.01}$
	O	-0.6093	$2s^{1.68}\ 2p^{4.90}\ 3p^{0.01}\ 3d^{0.02}$
$[Pt_3(\mu\text{-}CO)_3(PH_3)_3]$	Pt	-0.006	$6s^{0.64}\ 5d^{9.32}\ 7p^{0.02}$
	P	+0.276	$3s^{1.40}\ 3p^{3.25}\ 4s^{0.01}\ 3d^{0.05}\ 4p^{0.02}$
	C	+0.393	$2s^{1.31}\ 2p^{2.22}\ 3s^{0.03}\ 3p^{0.04}\ 3d^{0.01}$
	O	-0.628	$2s^{1.69}\ 2p^{4.91}\ 3p^{0.01}\ 3d^{0.02}$
Tl^+	Tl	+1.00	$5d^{10}\ 6s^2\ 6p^0$
Hg	Hg	0.00	$5d^{10}\ 6s^2\ 6p^0$

Table 8. Ionization Potential (I), Electron Affinity (A), Electronic Chemical Potential (m), Chemical Hardness (η), Global Electrophilicity Index (ω), Condensed Fukui function, local Electrophilicity Index at the platinum center. All values are in eV.

Cluster	Method	I	A	-m	η	ω	f^-_{Pt}	ω^-_{Pt}
$[Pt_3(\mu\text{-}CO)_3(PH_3)_3]$	HF	7.74	-0.91	3.41	4.33	1.34	0.212	0.284
	MP2	8.26	-0.54	3.86	4.40	1.69	0.202	0.341
	B3LYP	6.33	-2.59	4.46	1.87	5.32	0.221	1.176
	PBE	5.32	-3.07	4.19	1.12	7.84	0.241	1.889
$[Pt_3(\mu\text{-}SO)_3(PH_3)_3]$	HF	9.55	-1.25	5.40	4.15	3.51	0.169	0.593
	MP2	9.82	-1.62	5.72	4.10	3.99	0.158	0.630
	B3LYP	7.04	-3.89	5.46	1.57	9.49	0.248	2.353
	PBE	6.09	-4.22	5.16	0.94	14.16	0.289	4.090
$[Pt_3(\mu\text{-}CNH)_3(CNH)_3]$	HF	5.95	-1.00	2.48	3.48	0.88	0.190	0.168
	MP2	6.42	-0.98	2.72	3.70	0.99	0.167	0.167
	B3LYP	4.61	-1.31	2.96	1.65	2.66	0.165	0.438
	PBE	3.90	-1.94	2.92	0.98	4.35	0.159	0.692

CONCLUSION

The $[Pt_3(L)_3(L`)_3]$-MPH_3^+ (M = Au,Ag,Cu) complexes are stable at several levels of the theory. It is concluded that the equilibrium distances and interaction energies correspond essentially to an orbital interaction, in the magnitude of a covalent bond. The analysis of bonding and antibonding orbitals accounts for such interaction. It is possible to get different magnitudes in the interaction energies and Pt-M distances, depending on the type of ligands that form the Pt_3 core. The charge transfer is mainly due to the ligands, while platinum atoms and electrophiles receive charge. On the other hand, the $[Pt_3(L)_3(L`)_3]$-X (X = Hg, Tl^+) complexes describe a different behaviour than those described above. The mercury complex shows a metallophilic interaction of the dispersion term as the principal contribution in the stability. The thallium complex describes a strong metallophilic interaction due at the electrostatic and charge-induced

dipole terms. The local electrophilicity index on the platinum atoms (ω_{Pt}^-) allows finding the same sort of interaction energies: $[Pt_3(\mu\text{-}SO_2)_3(PH_3)_3] > [Pt_3(\mu\text{-}CO)_3(PH_3)_3] > [Pt_3(\mu\text{-}CNH)_3(CNH)_3]$.

ACKNOWLEDGEMENTS

This research was financed by FONDECYT under Project 1100162 (Conicyt-Chile), Project Millennium P07-006-F, and Basal Financing Program CONICYT-FB0807 (CEDENNA). Daniela Donoso has a National Doctoral Fellowship (Conicyt).

REFERENCES

1. F.F. de Biani, G. Manca, L. Marchetti, P. Leoni, S. Bruzzone, C. Guidotti, A. Atrei, A. Albinati, S. Rizzato, *Inorg. Chem.* **48**, 1385, (2009)
2. N.C. Payne, R. Ramachandran, G. Schoettel, J.J. Vittal, *Inorg. Chem.* **30**, 4048, (1991)
3. M. Baya, J. Houghton, D. Konya, Y. Champouret, J.C. Daran, K.Q.A. Lenero, L. Schoon, W.P. Mul, A.B. van Oort, N. Meijboom, E. Drent, A. Orpen, R. Poli, *J. Am. Chem. Soc.* **130**, 10612, (2008)
4. R. Ramachandran, R.J. Puddephatt, *Inorg. Chem.* **32**, 2256, (1993)
5. D. Imhof, L.M. Venanzi, Chem. *Soc. Rev.* **23**, 185, (1994)
6. A.D. Burrows, D.M.P. Mingos, *Coord. Chem. Rev.* **154**, 19, (1996)
7. A. Albinati, K.-H. Dahmen, F. Demartin, J.M. Forward, C.J. Longley, D.M.P. Mingos, L.M. Venanzi, *Inorg. Chem.* **31**, 2223 (1992)
8. D. Imhof, U. Burckhardt, K.-H. Dahmen, F. Joho, R. Nesper, *Inorg. Chem.* **36**, 1813, (1997)
9. P. Braunstein, J. Rosé in Stereochemistry of Organometallic and Inorganic Compounds. Vol III. Elsevier, Amsterdam, 1988.
10. A. Grushow, K.H. Ervin, *J. Am. Chem. Soc.* **117**, 11612, (1995)
11. D.I. Gilmour, D.M.P. Mingos, *J. Organometallic Chem.* **302**, 127, (1986)
12. D.M.P. Mingos, T.J. Slee, *J. Organometallic Chem.* **394**, 679, (1990)
13. D.G. Evans, *J. Organometallic Chem.* **352**, 397, (1988)
14. D. Donoso, F. Mendizabal, *Theor. Chem. Acc.* **129**, 381, (2011)
15. R.G. Parr, R.A. Donnelly, M. Levy, W.E. Palke, *J. Chem. Phys. 68*, 3801, (1978)
16. R.G. Parr, W. Yang in Density Functional Theory for atoms and molecules. Oxford Press: New York, 1989.
17. M. J. Frisch, G. W. Trucks, H. B. Schlegel, P. M. W. Gill, B. G. Johnson, M.A. Robb, J. R. Cheeseman, K. T. Keith, G. A. Petersson, J. A. Montgomery, K. Raghavachari, M. A. Al-Laham, V. G. Zakrzewski, J. V. Ortiz, J. B. Foresman, J. Cioslowski, B. B. Stefanov, A. Nanayakkara, M. Challacombe, C. Y. Peng, P. Y. Ayala, W. Chen, M. W. Wong, J. L. Andres, E. S. Replogle, R. Gomperts, R. L. Martin, D. J. Fox, J. S. Binkley, D. J. Defrees, J. Baker, J. P. Stewart, M. Head-Gordon, C. Gonzalez, J. A. Pople, Gaussian, Inc., Pittsburgh PA (USA), 2003.
18. C. Møller, M.S. Plesset, *Phys. Rev.* **46**, 618, (1934)
19. J.P. Perdew, K. Burke, M. Ernzerhof, *Phys. Rev. Letters* **77**, 3865, (1996)
20. D. Andrae, M. Heisserman, M. Dolg, H. Stoll, H. Preuss, *Theor. Chim. Acta* **77**, 123, (1990)
21. P. Pyykkö, F. Mendizabal, *Inorg. Chem.* **37**, 3018, (1998)
22. A. Bergner, M. Dolg, W. Küchle, H. Stoll, H. Preuss, *Mol. Phys.* **80**, 1431, (1993)
23. S. Huzinaga, *J. Chem. Phys.* **42**, 1293, (1965)
24. S.F. Boys, F. Bernandi, *Mol. Phys.* **19**, 553, (1970)
25. P.K. Chattaraj, D.R. Roy, *Chem. Rev.* **106**, 2065, (2006)
26. P.K. Chattaraj, B. Maiti, U. Sarkar, *J. Phys. Chem. A* **107**, 4973, (2003)
27. R.G. Parr, R.G. Pearson, *J. Am. Chem. Soc.* **105**, 7512, (1983)
28. R.G. Parr, L. von Szentpaty, S. Liu, *J. Am. Chem. Soc.* **121**, 1922, (1999)
29. R.G. Parr, R. Pearson, *J. Am. Soc. Soc.* **106**, 4049, (1984)
30. P. Pérez, R. Contreras, *Chem. Phys. Letters* **293**, 239, (1998)
31. R. Contreras, P. Fuentealba, M. Galván, P. Pérez, *Chem. Phys. Letters* **304**, 405, (1999)
32. P. Fuentealba, P. Pérez, R. Contreras, *J. Chem. Phys.* **113**, 2544, (2000)
33. F. Mendizabal, D. Donoso, D. Burgos, *Chem. Phys. Letters* **514**, 374, (2011)
34. D. Imhof, L.M. Venanzi, *Chem. Soc. Rev.* **23**, 185, (1994)
35. D. Imhof, K.-H. Burckhardt, H. Rüegger, T. Gerfin, G. Volker, *Inorg. Chem.* 32, 5206, (1993)
36. S.G. Bott, M. Hallam, O.J. Ezomo, D.M.P. Mingo, I.D. Williams, *J. Chem. Soc. Dalton Trans.* **4**, 1461, (1988)
37. D.M.P. Mingos, R.W.M. Wardle, *J. Chem. Soc. Dalton. Trans.* 1, 73, (1986)
38. J.E. Carpenter, F. Weinhold, *J. Mol. Struct.* **169**, *41*, (1988)
39. L. Hao, J.J. Vittal, R.J. Puddephatt, *Organometallic* 15, 3115, (1996)
40. A. Albinati, A. Moor, P.S. Pregosin, L.M. Venanzi, *J. Am. Chem. Soc.* **104**, 7672, (1982)
41. M. Green, A.K. Howard, M. Murray, J.L. Spencer, G.A. Stone *J. Chem. Soc. Dalton Trans.* **4**, 1509, (1977)